analytical chemistry

pubs.acs.org/ac Article

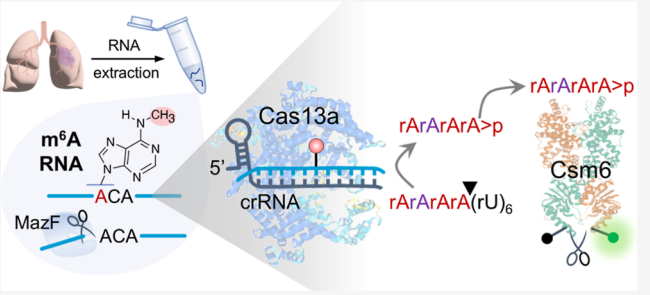
Preamplification-Free Detection of RNA N6-Methyladenosine Modification at Single-Base Resolution Using the CRISPR Tandem Assay

Kunyu Shi,[#] Yong Zhang,[#] Yiran Tao, Yuxi Wang, Jinliang Yang,[*] Ruijie Deng, and Hao Yang[*]

Cite This: https://doi.org/10.1021/acs.analchem.4c06782 Read Online

ACCESS | Metrics & More | Article Recommendations | Supporting Information

ABSTRACT: N6-Methyladenosine (m^6A) ranks among the most prevalent modifications in RNA, which serves as a biomarker for diseases, such as lung cancer. Herein, we developed a CRISPR/Cas13a-Csm6 tandem assay (termed CRISPRm^6A assay) allowing for preamplification-free, sensitive, and rapid detection of RNA m^6A modifications. The coupling of Cas13a-Csm6 tandem with MazF endoribonuclease enables the assay to identify m^6A RNA with single-base resolution. Compared to the CRISPRm^6A assay using Cas13a alone, the tandem CRISPRm^6A assay yielded an improved sensitivity for RNA detection by ∼22 times, thus enabling preamplification-free detection of RNA m^6A. Particularly, the proposed assay enabled quantification of m^6A abundance down to 0.5% at the picomole level in lncRNA MALAT1 and demonstrated a 100% correlation in diagnosing nonsmall cell lung cancer. In summary, the CRISPRm^6A assay supports two key applications in biological samples: (1) precise determination of m^6A sites and (2) quantitative measurement of m^6A fractions. Therefore, the CRISPR tandem method presents a promising tool for RNA epigenetics-based diagnostics.



INTRODUCTION

N6-Methyladenosine (m^6A), defined as the methylation occurring at the N6 position of adenosine, is the most abundant internal modification in eukaryotic mRNA.[1,2] RNA m^6A modification plays crucial roles in mRNA nuclear export, transcription, translation, splicing, and degradation, thus shaping the function of cells.[3−5] The abnormal level of RNA m^6A can contribute to human disorders and the occurrence of diseases such as lung cancers.[2,6,7] For example, METTL3-mediated m^6A modification of circRNA GF2BP3, FTO-regulated m^6A levels of USP7 mRNA, and a high concentration of m^6A in lncRNA MALAT1 promotes proliferation, invasion, and migration of nonsmall cell lung cancer.[8−10] Therefore, m^6A has gained attention as a promising biomarker for lung cancer diagnosis[11,12] and calls for the development of accurate and cost-effective tools for profiling RNA m^6A at single-base resolution.

RNA m^6A modification, currently, is profiled by liquid chromatography−mass spectrometry and sequencing. Liquid chromatography−mass spectrometry presents high sensitivity and accuracy but lacks the ability to achieve sequence resolution, resulting in the loss of genetic information.[13,14] Emerging high-throughput sequencing methods, often combined with m^6A pre-enrichment, provide detailed genetic information with single-base resolution.[15] Examples include antibody-based methylated RNA immunoprecipitation sequencing (MeRIP-seq)[16] and antibody-free FTO-assisted chemical labeling method (m^6A-SEAL).[17] However, the sequencing-based methods waste a large majority of their read capacity on nonclinically significant nucleotide information, increasing the time-, reagent- and data analysis-burden.[18] This limits their frequency of use in clinical applications, particularly in resource-limited regions. Recently, m^6A detection methods with single-base resolution leveraging RNA-modifying enzymes for recognition, such as MazF, RNase H, and DNA polymerase, have been developed.[19−21] For example, SELECT, a qPCR-based assay leveraging DNA polymerase and ligase for recognition, enables radiolabel-free and antibody-independent detection of site-specific m^6A modification with single-base resolution.[21] However, most of the above methods still rely on the preamplification of trace nucleic acid samples, which, inevitably leads to aerosol contamination risk, complexity increase, and high costs.[22−24] Particularly, the nonspecific or biased nucleic acid amplification can reduce their capacity to quantify RNA m^6A, thus compromising the precision for RNA m^6A-based diagnosis.

Received: December 14, 2024
Revised: May 16, 2025
Accepted: May 21, 2025

Downloaded via SHANGHAI NORMAL UNIV on May 26, 2025 at 01:47:44 (UTC).
See https://pubs.acs.org/sharingguidelines for options on how to legitimately share published articles.

© XXXX American Chemical Society

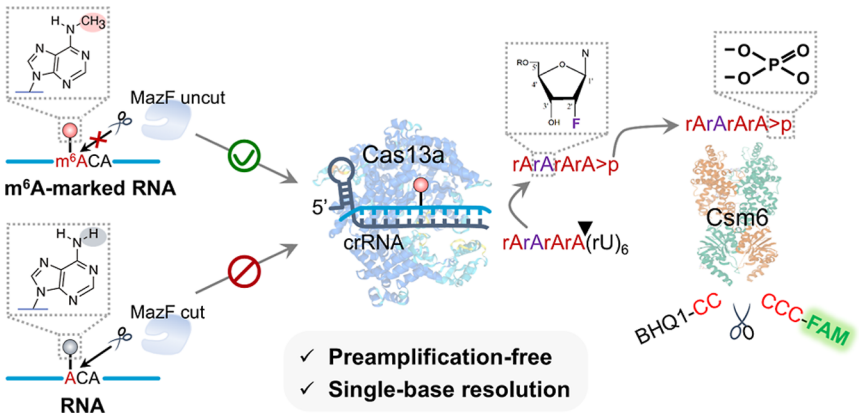


Figure 1. Working principle of the CRISPRm^{6}A assay for the detection of m^{6}A RNA. The m^{6}A modification on the "ACA" motif blocks MazF cleavage, resulting in an intact RNA oligonucleotide that can activate the subsequent turn-on signaling produced by the Cas13a-Csm6 tandem system. This assay enables preamplification-free detection of m^{6}A RNA with single-base resolution.

Herein, we develop an RNA methylation assaying method (termed CRISPRm^{6}A) that employs MazF to recognize the locus-specific m^{6}A and is coupled with the Cas13a-Csm6 tandem CRISPR system to amplify the recognition event. The dual recognition and cleavage processes involving MazF and CRISPR/Cas13a-Csm6 confer the CRISPRm^{6}A assay with single-base resolution and the ability to evade nucleic acid amplification. The CRISPRm^{6}A assay based on the Cas13a-Csm6 tandem system can achieve preamplification-free sensing of m^{6}A RNA with a detection limit of 0.56 pM, approximately 22 times more sensitive than the Cas13-only method. In addition, we employ the CRISPRm^{6}A assay to monitor the progression of nonsmall cell lung cancer, highlighting its potential as a diagnostic tool for RNA epigenetic alterations in early stage diseases. Overall, the CRISPRm^{6}A assay achieves two core functions benchmarked against SELECT[21]—accurately detects single m^{6}A sites and quantifies m^{6}A fractions in biological samples.

EXPERIMENTAL SECTION

Materials and Reagents. All DNA and RNA sequences (Table S1 in Supporting Information) were synthesized by Sangon Biotech (Shanghai, China) and purified by HPLC. New England Biolabs (Beijing, China) supplied dNTP mixtures (N0447S), T7 RNA polymerase (EP0111), NTP mixtures (R0481), and Phi29 DNA polymerase (EP0094). GelRed Dye (41001) was sourced from Biotium (Beijing, China). The mRNA Interferase-MazF, dNTP mixture (dNTPs), and RNase-free water was purchased from TaKaRa Biotechnology Co., Ltd. (Dalian, China).

Expressing and Purifying CRISPR Proteins. The plasmids containing DNA sequences that encode *Leptotrichia buccalis* Cas13a (LbuCas13a) and *Thermus thermophilus* Csm6 (TtCsm6)[25] were constructed and sequenced by Sangon Biotech (Shanghai, China). The sequences are listed in Table S2 (in Supporting Information). Next, the expression vectors corresponding to LbuCas13a and TtCsm6 were transformed into Rosetta2 DE3 strains and cultured in LB medium at 37 °C. Then, mid log phase cultures were treated with 0.5 mM IPTG (isopropyl-β-D-thiogalactopyranoside) to induce expression, which was carried out overnight at 16 °C. The cells were precipitated and harvested, then resuspended in lysis buffer (for LbuCas13a: 500 mM NaCl, 50 mM HEPES, pH = 7.0, 0.5 mM PMSF, 1 mM TCEP, 10% glycerol, and EDTA-free protease inhibitor; for TtCsm6:500 mM KCl, 20 mM HEPES, pH = 8.0, 1 mM TCEP, and 5 mM imidazole, enriched with EDTA-free protease inhibitors from TaKaRa), and lysed by an experimental high-pressure homogenizer. Postcentrifugation, the supernatant was combined with a HiTrap Ni-NTA column (GE Healthcare) at 4 °C for binding. Following buffer washing, elution of the target protein was carried out using a lysis buffer containing a linear gradient of imidazole concentrations ranging from 0.01 to 0.3 M. Eluted proteins were dialyzed overnight using the storage buffer (for LbuCas13a: 200 mM KCl, 1 mM TCEP, 20 mM HEPES (pH = 7.0), and 10% glycerol; for TtCsm6:150 mM NaCl, 1 mM TCEP, 25 mM HEPES (pH = 7.5), and 5% glycerol) in the presence of tobacco etch virus protease. Flow-through fractions were obtained after passing the dialyzed proteins through the Ni-NTA cartridge and further purification by size exclusion chromatography on a Superdex 200 16/600 column from GE Healthcare in storage buffer. Fractions at the peak of elution were collected and concentrated (Amicon Ultra Centrifugal Filter) to achieve a concentration range of 15−50 mg/mL. Finally, the purified proteins were analyzed by SDS-PAGE (NuPAGE Bis-Tris 4−12%, Invitrogen) and Coomassie blue staining, as shown in Figures S1 and S2 in Supporting Information. Subsequently, the purified proteins were flash-frozen in liquid nitrogen and stored at −80 °C.

CRISPRm^{6}A Assay for m^{6}A Detection. The CRISPRm^{6}A detection involves two steps, including MazF cleavage and CRISPR signaling. First, the MazF cleavage was conducted in a 20 μL reaction volume containing 5× MazF buffer, mRNA Interferase-MazF, and various concentrations of RNA samples to be tested, incubated at 37 °C for 15 min. Subsequently, the CRISPR signaling was conducted in a 40 μL reaction volume, which contained 4 μL of the above mixture, 4 μL of Cas13a buffer (5 mM $MgCl_2$, 20 mM HEPES (pH = 6.8), 5% glycerol, and 50 mM KCl), 4 μL of Cas13a (1 μM), 4 μL of Csm6 (2 μM), 4 μL of crRNA (1 μM), 4 μL of F-rA_4-rU_6 activator (10 μM), 4 μL of C5 reporter (4 μM), and 12 μL of DEPC-treated water. The CRISPR signaling mixture was incubated at 37 °C for 45 min. The fluorescence output was ultimately measured using a Synergy H1 microplate reader (BioTek, USA), with an excitation wavelength of 480 nm and emission detected between 510 and 600 nm.

To quantify the m^{6}A fraction, a standard curve was constructed using synthesized 0−20% m^{6}A RNA at a final

https://doi.org/10.1021/acs.analchem.4c06782
Anal. Chem. XXXX, XXX, XXX−XXX

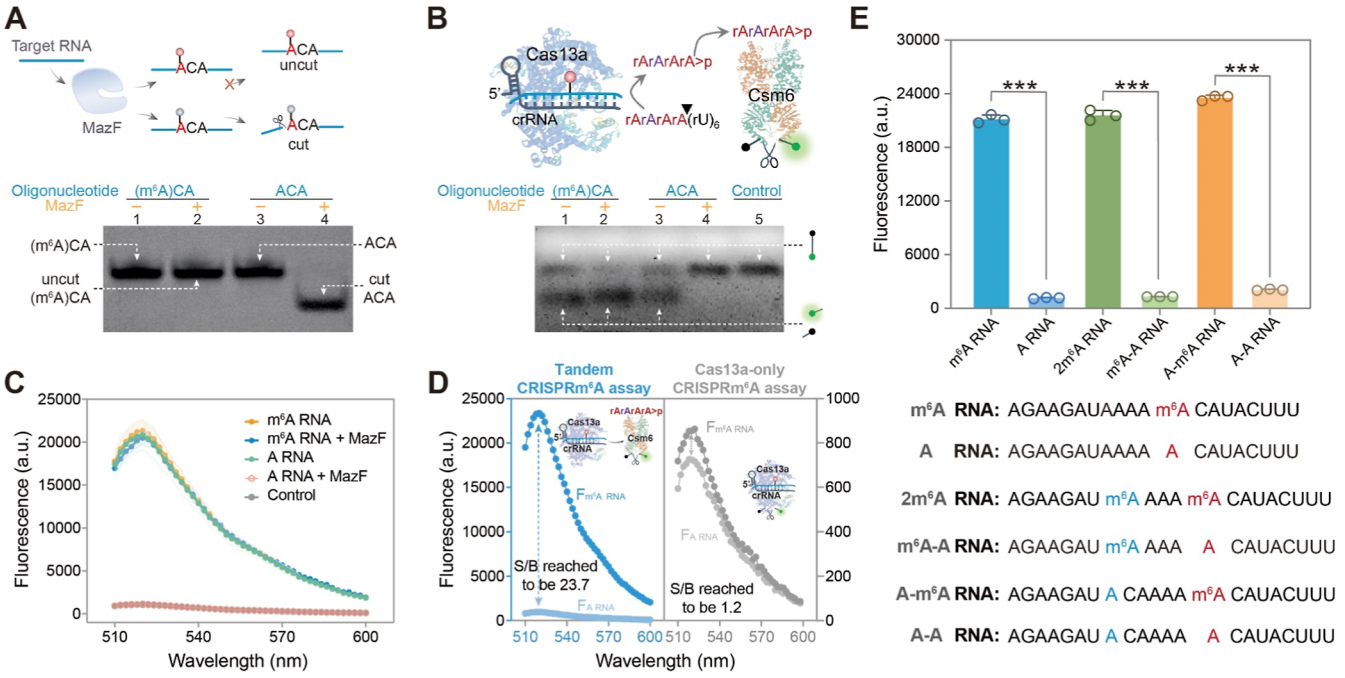


Figure 2. Investigation of the mechanism underlying the CRISPRm^{6}A assay for locus-specific detection of m^{6}A modifications in RNA. (A) Electrophoresis analysis of the MazF cutting for m^{6}A recognition. (B) Electrophoresis analysis of the tandem CRISPR cleavage of C5 reporter. (C) Fluorescence analysis of the CRISPRm^{6}A assay toward m^{6}A RNA. (D) Fluorescence response of the CRISPRm^{6}A assay using tandem Cas13a-Csm^{6}And lonely Cas13a. (E) Fluorescence analysis of the CRISPRm^{6}A assay was performed using RNA oligonucleotides containing either two m^{6}A sites or two unmodified "ACA" motifs. The excitation and emission wavelengths were 480 nm and 510−600 nm, respectively. The concentrations of target RNA, MazF, Cas13a nuclease, crRNA, rA$_4$-rU$_6$, Csm6 nuclease, and C5 reporter were 1 nM, 2 U/μL, 100 nM, 100 nM, 1 μM, 200 nM, and 400 nM, respectively. Two-tailed Student's t-test was carried out: ***$P < 0.001$.

concentration of 1 nM, which correlates the m^{6}A fraction with fluorescence intensity. This curve was then used to quantify the m^{6}A contents in both the cancerous and pericarcinomatous tissues of lung cancer patients. In particular, for the samples with m^{6}A content exceeding 20%, gradient dilution was applied before measurement and the actual content was determined by recalculating from the diluted concentration.

RESULTS AND DISCUSSION

Working Principles. The CRISPRm^{6}A assay involves two sequential procedures: (i) MazF cutting for m^{6}A recognition and (ii) tandem CRISPR cleavage for signal amplification (Figure 1). RNA m^{6}A sites are typically located in sequence contexts like RRACH (where R = A/G and H = A/C/U), with the majority featuring the "ACA" motif. As a result, we used MazF as a model endonuclease to test the feasibility of the CRISPRm^{6}A assay. The m^{6}A-sensitive endoribonuclease MazF specifically recognizes the "ACA" motif and precisely cleaves at its 5′-end, however, methylation at the first adenine—forming (m^{6}A)CA—effectively blocks this cleavage. This feature highlights the proficiency of MazF in recognizing m^{6}A-modified RNA sequences. The resultant intact "(m^{6}A)CA" sequence was a key activator for the CRISPR/Cas13a-Csm6 tandem endoribonuclease, initiating CRISPR-mediated signaling. LbuCas13a preferentially cleaves homouridine substrates (polyU), with minimal cleavage activity observed on homoadenosine substrates (polyA).[26] Therefore, crRNA-guided activated LbuCas13a[27] can specifically cut the rA$_4$-rU$_6$ oligonucleotide, generating rA$_4$ > p terminated with 2′,3′-cyclic phosphate capable of activating the subsequent Csm6 cleavage, resulting in cascade amplification of fluorescence signals. Given that cytidine homopolymers serve as potent activators of Csm6-mediated trans-cleavage, we designed a Csm6-specific reporter—termed the C5 reporter—consisting of a polyC sequence labeled with a fluorophore at the 5′ end and a quencher at the 3′ end. This reporter enables the monitoring of Csm6 cleavage activity within the CRISPR/Cas system, offering a high sensitivity and amplification-free method for the detection of RNA m^{6}A modifications.

The m^{6}A-specific MazF cutting and tandem CRISPR cleavage were first visually verified by using electrophoresis. The oligonucleotide containing the "(m^{6}A)CA" motif retained the full length in the presence of MazF endoribonuclease, whereas the band corresponding to the "ACA" oligonucleotide (lane 4) completely disappeared, highlighting the m^{6}A-specific cutting activity of MazF (Figure 2A). The full-length oligoribonucleotides, regardless of whether they carry the m^{6}A modification, activate the tandem CRISPR cleavage, as evidenced by the forward migration of the band loaded with abundant C5 reporters. The absence of the m^{6}A modification, which resulted in the cleavage of the "ACA" oligoribonucleotide, caused the band to show minimal change compared with the control. These observations demonstrated the ability of the tandem CRISPR system to process and amplify the MazF cutting event, resulting in a detectable signal output (Figure 2B). Fluorescence analysis was subsequently performed to evaluate the CRISPRm^{6}A assay for identification of m^{6}A modification (Figure 2C). Minimal increases in fluorescence intensity occurred when the RNA containing the "ACA" motif was cut by MazF compared to the blank fluorescence of the reporter alone. However, a significant fluorescence enhancement was observed in the presence of m^{6}A modification, regardless of MazF cleavage, with the fluorescence intensity nearly matching that of the positive control using full-length

https://doi.org/10.1021/acs.analchem.4c06782
Anal. Chem. XXXX, XXX, XXX−XXX

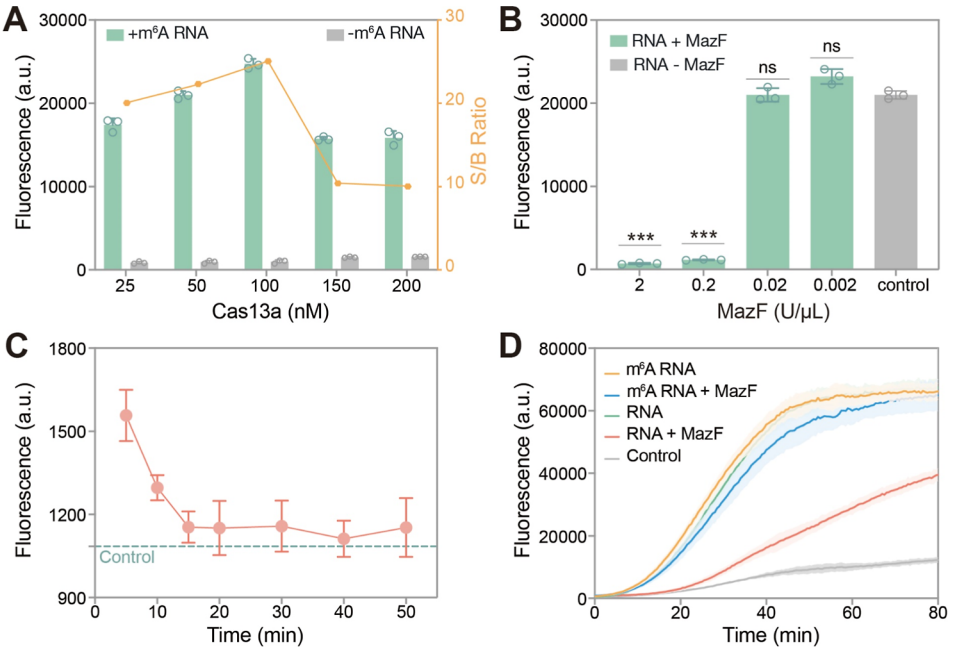


Figure 3. Optimization of the CRISPRm^{6}A assay. (A,B) Fluorescence output and the S/B ratio of the CRISPRm^{6}A assay response to m^{6}A RNA using different concentrations of Cas13a and Csm6 nucleases. (C,D) Fluorescence output and the S/B ratio of the CRISPRm^{6}A assay response to m^{6}A RNA using different reaction times of MazF cutting and tandem CRISPR cleavage. The excitation and emission wavelengths were 480 nm and 510−600 nm, respectively. Two-tailed Student's *t*-test was carried out: ***$P < 0.001$, ns, $P > 0.05$.

RNA. Furthermore, we conducted a comparison to assess the signaling efficacy of Cas13a-Csm6 in tandem versus Cas13a alone (Figure 2D). Cas13a and Csm6 exhibit distinct cleavage preferences (polyU for Cas13a and polyC for Csm6), with Cas13a unable to process the polyC reporter (Figure S3 in Supporting Information). We thus selected reporters that align with the specific cleavage preferences of Cas13a and Csm6. The employment of Cas13a-Csm6 presented a 23.7-fold enhancement in the signal-to-background ratio (S/B ratio) compared to the independent use of Cas13a, indicating that tandem CRISPR is capable of signal amplification.

In addition, to investigate the feasibility of this method to detect m^{6}A at single-base resolution, we tested RNA oligonucleotides containing various combinations of m^{6}A and ACA sites (2m^{6}A, m^{6}A−A, A-m^{6}A, and A−A RNA). Given that the central region of the crRNA spacer, known as the seed region, is the most sensitive to mismatches,[28] the target (m^{6}A)CA site was thus positioned within this seed region. An adjacent m^{6}A modification was shown to have little impact on the detection of the target (m^{6}A)CA site, confirming that MazF cleavage remains unaffected, highlighting the single-base resolution of the CRISPRm^{6}A assay (Figure 2E). Similarly, the presence of an additional adjacent ACA motif did not compromise the assay performance, likely due to its positioning outside the seed region of the crRNA spacer (Figure 2E).

Optimization of the CRISPRm^{6}A Assay. The CRISPRm^{6}A assay hinges on the efficacy of m^{6}A recognition by MazF and the subsequent tandem CRISPR cleavage. We first investigated the sequence preference of Cas13a cleavage, and the result showed that sequence T3 enabled the production of the highest assaying signal (Figure S4 in Supporting Information). And, we further investigated the impact of Cas13a and MazF concentrations on the CRISPRm^{6}A assay (Figure 3A,B). The highest fluorescence output was achieved with a Cas13a concentration of 100 nM and a MazF concentration of 0.2 U/μL, while maintaining a low-level background. The reaction time of MazF cutting and tandem CRISPR cleavage is another crucial factor, as it significantly influences the efficiency and precision of the proposed CRISPRm^{6}A assay. As revealed in Figure 3C,D, MazF cutting would achieve a maximum after 15 min, as indicated by the fluorescence approaching that of the blank control, followed by tandem CRISPR cleavage, which reached equilibrium within 45 min. The fluorescence response to MazF cutting, approaching the blank control, and to CRISPR cleavage, nearly matching the positive control without MazF, highlighted the high catalytic cleavage efficiency.

Quantification of RNA m^{6}A Methylation. Upon the optimal sensing conditions, a series of synthetic m^{6}A RNA amounts were used to assess the quantification performance of the CRISPRm^{6}A assay, with the assay using Cas13a alone as a comparison. Fluorescence signals gradually increased in both assays as the amount of m^{6}A RNA was elevated (Figures 4 and S5 in Supporting Information). A linear regression equation ($Y = 569.6X + 784.3$, $R^2 = 0.9913$) for the tandem CRISPRm^{6}A assay was observed (Figure 4A), showing a strong correlation between the fluorescence signal (Y) and m^{6}A RNA concentration (X) in the range of 0 to 40 pM, with a high correlation coefficient (R^2) of 0.9913. The limit of detection (LOD) was defined as the m^{6}A RNA concentration that generated a fluorescence signal 3 times the standard deviation of the minimum within the linear range. With the benefit of signal amplification via tandem CRISPR cleavage, the CRISPRm^{6}A assay could detect m^{6}A RNA at a subpicomolar level of LOD, reaching as low as 0.56 pM. In contrast, the Cas13a-only CRISPRm^{6}A assay presented an LOD of 12.50 pM (Figure 4B), approximately 22-fold higher than the tandem CRISPRm^{6}A assay (Figure 4C). Furthermore, the proposed assay was challenged to differentiate m^{6}A RNA from unmodified ones. A series of m^{6}A RNA mixtures with defined modification

https://doi.org/10.1021/acs.analchem.4c06782
Anal. Chem. XXXX, XXX, XXX−XXX

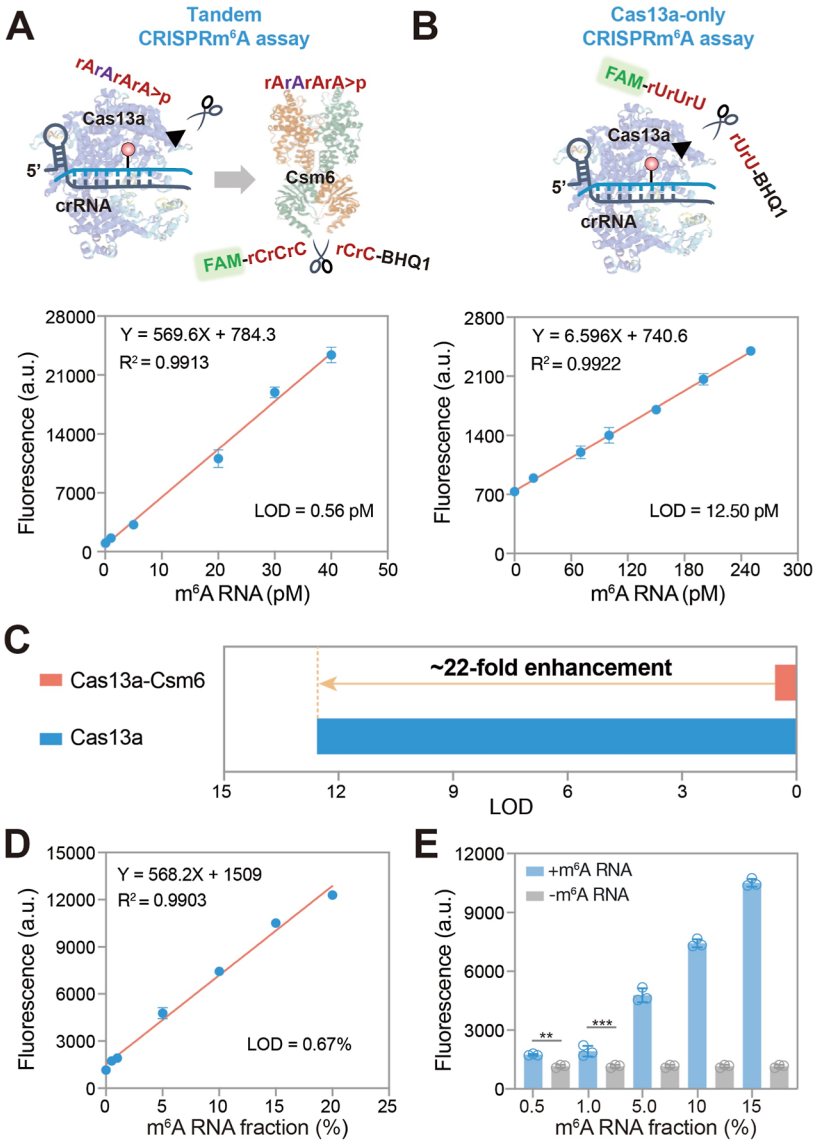


Figure 4. Quantification performance of the CRISPRm^{6}A assay. Linear relationship between the m^{6}A RNA concentrations and the corresponding fluorescence output of the (A) tandem CRISPRm^{6}A assay and (B) Cas13a-only CRISPRm^{6}A assay. (C) Comparisons of the LODs for both CRISPRm^{6}A assays. (D) Linear relationship between the m^{6}A RNA fractions and the corresponding fluorescence output of the tandem CRISPRm^{6}A assay. (E) Fluorescence responses of the tandem CRISPRm^{6}A assay toward different fractions of m^{6}A RNA. Two-tailed Student's *t*-test was carried out: ***$P < 0.001$, **$P < 0.01$.

fractions (0−20%) at a total RNA concentration of 1 nM were prepared and used to assess the quantification performance of the CRISPRm^{6}A assay. The linear calibration curve for detecting m^{6}A RNA was determined to be $Y = 568.2X + 1509$, with an R^2 value of 0.9903 and a theoretical LOD of 0.67% (Figure 4D). However, the proposed assay demonstrated the ability to effectively detect the abundance of m^{6}A RNA at a level as low as 0.5% (Figure 4E). Leveraging tandem signal amplification, the CRISPRm^{6}A assay eliminates the need for nucleic acid amplification, offering reduced assaying time (Table S3 in Supporting Information).

Analysis of the m^{6}A Level in Lung Cancer Tissues. MALAT1 lncRNA frequently undergoes m^{6}A methylation and serves as a key regulator in lung cancer metastasis, influencing processes like cell migration and invasion.[29,30] Its dysregulation enhances the metastatic potential of lung cancer cells.[31,32] Consequently, we further applied the CRISPRm^{6}A assay to analyze the m^{6}A modification levels in the MALAT1 lncRNA of clinical lung cancer tissues (Figure 5A). A total of 24 lung tissue samples, including 12 cancerous and 12 corresponding pericarcinomatous tissues, were ethically collected from the West China Hospital, Sichuan University. The prepared tissue samples were analyzed using the CRISPRm^{6}A assay and parallelly compared with clinical diagnosis. The CRISPRm^{6}A assay accurately identified the cancerous status in 23 out of 24 samples, with only one instance of false-negative result and no false-positive outcome (Figure S6 in Supporting Information). We found that MALAT1 expression levels are comparable between pericarcinomatous tissues and cancerous tissue samples (Figures 5B and S7 in Supporting Information), suggesting that MALAT1 expression has a minimal impact on the abundance of m^{6}A modification. A significant difference in fluorescence output was observed, with the cancerous tissue samples showing notably higher signal values compared to the pericarcinomatous tissues. And, the m^{6}A modification level in cancerous tissues was at least 5.04%, with the highest reaching

https://doi.org/10.1021/acs.analchem.4c06782
Anal. Chem. XXXX, XXX, XXX−XXX

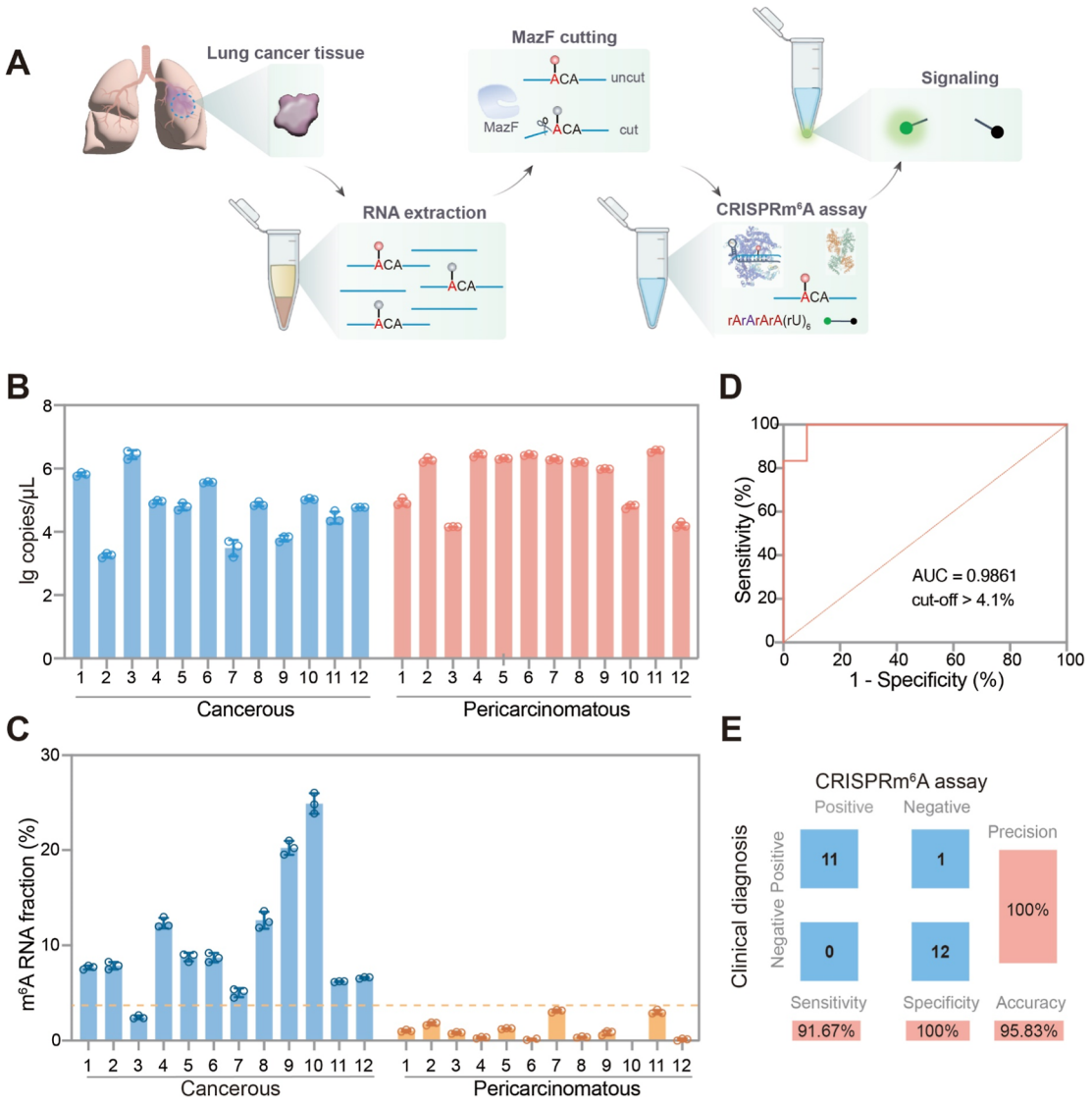


Figure 5. Practical application of the CRISPRm^{6}A assay for detecting the m^{6}A modification level in clinical lung cancer samples. (A) Scheme for the assaying protocol of m^{6}A RNA in the MALAT1 gene of clinical lung tissues. (B) MALAT1 expression levels in 12 cancerous tissue samples and 12 pericarcinomatous tissue samples. (C) Fluorescence responses of the CRISPRm^{6}A assay toward different m^{6}A RNA fractions. (D) ROC analysis of assaying sensitivity and specificity of the CRISPRm^{6}A assay. (E) Confusion matrix analysis of 12 cancer and 12 pericarcinomatous tissue samples.

24.90%, significantly higher than that in pericarcinomatous tissues (Figure 5C). The receiver operating characteristic (ROC) curve analysis showed an area under the curve (AUC) of 0.9861 (Figure 5D). Moreover, the confusion matrix analysis revealed that the CRISPRm^{6}A assay exhibited analytical sensitivity and specificity of 91.67% and 100%, respectively (Figure 5E). Both results demonstrated a strong correlation between the CRISPRm^{6}A assay and the clinically diagnosed outcomes. Additionally, to assess the risk of nonspecific signaling from complex clinical matrices, we used two randomized RNAs—A RNA_{rd} and m^{6}A-RNA_{rd}—containing ACA or (m^{6}A)CA motifs, respectively, as controls in m^{6}A-free samples. Fluorescence signals remained stable after adding pericarcinomatous tissue lysate extracts (Figure S8 in Supporting Information), confirming the specificity and robustness of the CRISPRm^{6}A assay in complex biological matrices. These findings highlight the potential of the CRISPRm^{6}A assay as a reliable method for the accurate determination of m^{6}A sites and quantification of m^{6}A fractions in biological samples such as cancer tissues.

CONCLUSIONS

In summary, we developed a cascade CRISPR assay (termed CRISPRm^{6}A assay) using Cas13a in tandem with Csm6 for sensitive detection of m^{6}A modifications in lung cancer tissues. The Cas13a-Csm6 in tandem exhibited ~22-fold signal amplification compared to the Cas13a-only CRISPRm^{6}A assay, enabling preamplification-free m^{6}A RNA detection with a detection limit of 0.56 pM. In addition, dual recognition using MazF and CRISPR endowed the proposed assay with high specificity at the single-base level. Particularly, the CRISPRm^{6}A assay enabled the detection of m^{6}A RNA in lncRNA MALAT1 of lung cancer tissues at abundances as low as 0.5%, highlighting its potential as a promising tool for diagnosing RNA epigenetic-associated diseases.

https://doi.org/10.1021/acs.analchem.4c06782
Anal. Chem. XXXX, XXX, XXX−XXX

■ ASSOCIATED CONTENT

Supporting Information

The Supporting Information is available free of charge at https://pubs.acs.org/doi/10.1021/acs.analchem.4c06782.

Experimental procedures; oligonucleotide sequences; gene sequences of LbuCas13a and TtCsm6; comparison of detection performance of different assays for m^{6}A detection; SDS-PAGE analysis of purified LbuCas13a protein; SDS-PAGE analysis of purified TtCsm6 protein; comparison of the detection performance of the Cas13a-only CRISPRm^{6}A assay using U5 and C5 reporter; sequences screened to align with the established specificity of Cas13a for targeted cleavage; investigation of the quantification performance for m^{6}A RNA detection; practical application of the CRISPRm^{6}A assay for detecting the m^{6}A modification level in clinical lung samples; quantification of MALAT1 expression levels in the clinical tissue samples; and investigation of the impact of complex clinical matrices on the m^{6}A detection using the CRISPRm^{6}A assay (PDF)

■ AUTHOR INFORMATION

Corresponding Authors

Jinliang Yang − *State Key Laboratory of Biotherapy and Cancer Center/Collaborative Innovation Center for Biotherapy, Department of Pulmonary and Critical Care Medicine, Targeted Tracer Research and Development Laboratory, Institute of Respiratory Health, West China Hospital, Sichuan University, Chengdu 610041, China;* orcid.org/0000-0002-6152-6394; Email: jinliangyang@scu.edu.cn

Hao Yang − *College of Biomass Science and Engineering and School of Chemical Engineering, Sichuan University, Chengdu 610065, China;* orcid.org/0009-0007-7421-3200; Email: hyang23@scu.edu.cn

Authors

Kunyu Shi − *State Key Laboratory of Biotherapy and Cancer Center/Collaborative Innovation Center for Biotherapy, Department of Pulmonary and Critical Care Medicine, Targeted Tracer Research and Development Laboratory, Institute of Respiratory Health, West China Hospital, Sichuan University, Chengdu 610041, China*

Yong Zhang − *College of Biomass Science and Engineering, Sichuan University, Chengdu 610065, China*

Yiran Tao − *West China-California Research Center for Predictive Intervention Medicine, West China Hospital, Sichuan University, Chengdu 610041, China*

Yuxi Wang − *State Key Laboratory of Biotherapy and Cancer Center/Collaborative Innovation Center for Biotherapy, Department of Pulmonary and Critical Care Medicine, Targeted Tracer Research and Development Laboratory, Institute of Respiratory Health, West China Hospital, Sichuan University, Chengdu 610041, China; Frontiers Medical Center, Tianfu Jincheng Laboratory, Chengdu 610212, China;* orcid.org/0000-0002-4056-5829

Ruijie Deng − *College of Biomass Science and Engineering, Sichuan University, Chengdu 610065, China;* orcid.org/0000-0001-9094-124X

Complete contact information is available at: https://pubs.acs.org/10.1021/acs.analchem.4c06782

Author Contributions

#K.S. and Y.Z. contributed equally to this work.

Notes

The authors declare no competing financial interest.

■ ACKNOWLEDGMENTS

This work was financially supported by National Key Research and Development Program of China (2022YFF1103000), National Natural Science Foundation of China (22074100), Postdoctoral Fellowship Program of CPSF (GZC20231774), Natural Science Foundation of Sichuan (2025ZNSFSC1041), and Chengdu Science and Technology Support Program (2024-YF05-00697-SN).

■ REFERENCES

(1) Zong, D.; Oberdoerffer, P.; Batista, P. J.; Nussenzweig, A. *Nat. Rev. Gene.* **2020**, *21* (11), 651−670.
(2) Jiang, X.; Liu, B.; Nie, Z.; Duan, L.; Xiong, Q.; Jin, Z.; Yang, C.; Chen, Y. *Signal Transduction Targeted Ther.* **2021**, *6* (1), 74.
(3) Yang, C.; Hu, Y.; Zhou, B.; Bao, Y.; Li, Z.; Gong, C.; Yang, H.; Wang, S.; Xiao, Y. *Cell Death Dis.* **2020**, *11* (11), 960.
(4) Lee, Y.; Choe, J.; Park, O. H.; Kim, Y. K. *Trends Genet.* **2020**, *36* (3), 177−188.
(5) Zhang, T.; Yang, H.; Yu, Q.; Zhang, Y.; Zhang, Y.; Zhu, X.; Xia, X.; Li, F.; Deng, R. *Angew. Chem., Int. Ed.* **2025**, *64* (9), No. e202418003.
(6) Sun, T.; Wu, R.; Ming, L. *Biomed. Pharmacother.* **2019**, *112*, 108613.
(7) Liu, Z.; Gao, L.; Cheng, L.; Lv, G.; Sun, B.; Wang, G.; Tang, Q. *Exp. Mol. Med.* **2023**, *55* (3), 487−501.
(8) Liu, Z.; Wang, T.; She, Y.; Wu, K.; Gu, S.; Li, L.; Dong, C.; Chen, C.; Zhou, Y. *Mol. Cancer* **2021**, *20* (1), 105.
(9) Roh, J.; Kim, B.; Im, M.; Jang, W.; Chae, Y.; Kang, J.; Youn, B.; Kim, W. *BMC Cancer* **2023**, *23* (1), 818.
(10) Yin, H.; Chen, L.; Piao, S.; Wang, Y.; Li, Z.; Lin, Y.; Tang, X.; Zhang, H.; Zhang, H.; Wang, X. *Cell Death Differ.* **2023**, *30* (3), 605−617.
(11) Weber, D. G.; Johnen, G.; Casjens, S.; Bryk, O.; Pesch, B.; Jöckel, K. H.; Kollmeier, J.; Brüning, T. *BMC Res.* **2013**, *6*, 518.
(12) Shen, L.; Chen, L.; Wang, Y.; Jiang, X.; Xia, H.; Zhuang, Z. *J. Neurooncol.* **2015**, *121* (1), 101−108.
(13) Li, L.; Hao, X.; Chen, H.; Wang, L.; Chen, A.; Song, X.; Hu, Z.; Su, Y.; Lin, H.; Fan, P. *Biomed. Chromatogr.* **2020**, *34* (9), No. e4897.
(14) Lü, C.; Xu, H.; Gao, P.; Huang, A.; Qu, M.; He, W.; Wu, H.; Chen, J.; Xu, B.; Guo, L.; et al. *Anal. Chem.* **2024**, *96* (18), 6870−6874.
(15) Dominissini, D.; Moshitch-Moshkovitz, S.; Schwartz, S.; Salmon-Divon, M.; Ungar, L.; Osenberg, S.; Cesarkas, K.; Jacob-Hirsch, J.; Amariglio, N.; Kupiec, M.; et al. *Nature* **2012**, *485* (7397), 201−206.
(16) Ye, H.; Li, T.; Rigden, D. J.; Wei, Z. *Nucleic Acids Res.* **2024**, *52* (9), 4830−4842.
(17) Wang, Y.; Xiao, Y.; Dong, S.; Yu, Q.; Jia, G. *Nat. Chem. Bio.* **2020**, *16* (8), 896−903.
(18) McIntyre, A. B. R.; Gokhale, N. S.; Cerchietti, L.; Jaffrey, S. R.; Horner, S. M.; Mason, C. E. *Sci. Rep.* **2020**, *10* (1), 6590.
(19) Zhong, K.; Wu, Y.; Zhou, J.; Yang, X.; Yi, C.; Ge, L.; Li, Z.; He, W.; Cao, J.; Jiang, G.; et al. *Anal. Chem.* **2023**, *95* (51), 18821−18827.
(20) Ma, X.; Xia, Y.; Wang, S.; Yang, Z.; Lei, X.; Wu, Y.; Gao, X.; Ren, X. *Anal. Chem.* **2023**, *95* (48), 17595−17602.
(21) Xiao, Y.; Wang, Y.; Tang, Q.; Wei, L.; Zhang, X.; Jia, G. *Angew. Chem., Int. Ed.* **2018**, *57* (49), 15995−16000.
(22) Wei, L.; Wang, Z.; Wu, L.; Chen, Y. *Biosens. Bioelectron.* **2023**, *222*, 114984.
(23) Wu, Z.; Chen, Y.; Wei, J.; Deng, Y.; Deng, R.; Yang, H. *Biosens. Bioelectron.* **2024**, *266*, 116715.

(24) Yang, H.; Chen, J.; Yang, S.; Zhang, T.; Xia, X.; Zhang, K.; Deng, S.; He, G.; Gao, H.; He, Q.; et al. *Anal. Chem.* **2021**, *93* (37), 12602−12608.
(25) Yang, H.; Li, F.; Xue, T.; Khan, M. R.; Xia, X.; Busquets, R.; Gao, H.; Dong, Y.; Zhou, W.; Deng, R. *Anal. Chem.* **2022**, *94* (48), 16953−16959.
(26) East-Seletsky, A.; O'Connell, M. R.; Burstein, D.; Knott, G. J.; Doudna, J. A. *Mol. Cell* **2017**, *66* (3), 373−383.
(27) Du, L.; Zhu, Q.; Lin, Z. *EMBO J.* **2024**, *43* (2), 304−315.
(28) Yang, H.; Patel, D. J. *Nat. Chem. Biol.* **2024**, *20* (6), 673−688.
(29) Tano, K.; Mizuno, R.; Okada, T.; Rakwal, R.; Shibato, J.; Masuo, Y.; Ijiri, K.; Akimitsu, N. *FEBS Lett.* **2010**, *584* (22), 4575−4580.
(30) Mishra, A.; Mishra, S. *ACS Omega* **2024**, *9* (41), 42212−42226.
(31) Schmidt, L. H.; Spieker, T.; Koschmieder, S.; Humberg, J.; Jungen, D.; Bulk, E.; Hascher, A.; Wittmer, D.; Marra, A.; Hillejan, L.; et al. *J. Thorac. Oncol.* **2011**, *6* (12), 1984−1992.
(32) Wang, D.; Zhang, S.; Zhao, M.; Chen, F. *Cancer Med.* **2020**, *9* (23), 9138−9149.

https://doi.org/10.1021/acs.analchem.4c06782
Anal. Chem. XXXX, XXX, XXX−XXX